variation of P_{min} with thickness is shown in Figure 7(b) at 0 V. P_{min} is improved, that is lowered with the increases in d. At larger d, the NEB is transit-time limited, and so the effect of confinement becomes significant. It may be seen that the effect of confinement is to deteriorate the P_{min} except for a smaller diameter (e.g., 25 μm) and a smaller thickness (around 1 μm) when the confinement improves the minimum detectable power.

5. CONCLUSIONS

We have calculated the noise currents in a Ge-based schottky PD considering the carrier confinement effect at the Si/Ge heterointerface. The model results have been verified with experimental data taken from literature. We see that the noise equivalent BW of the detector is low at low bias because of the recombination of holes during confinement at the Si/Ge heterointerface. For high enough bias, the confinement is absent and the NEB reaches a constant value. The NEB/BW ratio indicates that there may be existing choice of thickness for which noise performance can be improved without affecting its high-frequency performance. We see that in the noise performance, the shot noise due to photocurrents and the thermal noise are mainly significant in the noise performance of the PD. Results on S/N ratio and minimum detectable power show that the effective noise current increases with bias and thickness. At low bias and large thicknesses, the effect of heterointerface confinement of holes is significant. The heterointerface confinement improves the noise performance of a PD having small dimensions (where the RC effect is not significant) and operated at low bias.

ACKNOWLEDGMENTS

The authors wish to acknowledge the help of their colleagues in the department of Radio Physics and Electronics and A. K. Choudhury School of Information Technology, University of Calcutta.

REFERENCES

1. G. Keiser, Optical Fiber Communications, McGraw-Hill Int., Singapore, 1989.
2. N.R. Das, Y.M. El-Batawy, and M.J. Deen, In: M.J. Deen, D. Misra, and J. Ruzyllo (Eds.), Integrated Optoelectronics, Vol. PV 2002-4, The ElectroChemical Society Inc., New Jersy, 2002, p. 163.
3. J.-W. Shi, H.-C. Hsu, F.-H. Huang, W.-S. Liu, J.-I. Chyi, J.Y. Lu, C.-K. Sun, and C.-L. Pan, Separated-transport-recombination p-i-n Photodiode for High-speed and High-power Performance, IEEE Photon Technol Lett 17 (2005), 1722.
4. Y. Sekiguchi, T. Kuwahara, F. Kobayashi, and S. Iio, 34 GHz bandwidth GaAs high-speed schottky barrier photodiode fabricated by chemical-beam epitaxy, Jpn J Appl Phys 31 (1992), L180.
5. W.A. Wohlmuth, J.-W. Seo, P. Fay, C. Caneau, and I. Adesida, A high-speed ITO–InAlAs–InGaAs Schottky-barrier photodetector, IEEE Photon Technol Lett 9 (1997), 1388.
6. M. Salib, L. Liao, R. Jones, M. Morse, A. Liu, D. Samara-Rubio, D. Alduino, and M. Paniccia, Silicon photonics, Intel Technol J 8 (2004), 143.
7. S.M. Csutak, J.D. Schaub, B. Yang, and J.C. Campbell, High-speed short-wavelength silicon photodetectors fabricated in 130-nm CMOS process, Proc SPIE Photon Packag Integr III 4997 (2003), 135.
8. N.R. Das and M.J. Deen, SiGe and SiGeC-Based Devices for Si-Based Photonics, IWPSD-2003, Indian Institute of Technology Madras, Chennai, India, 2003.
9. M. Ghioni, F. Zappa, V.P. Kesan, and J. Warnock, A VLSI-compatible high-speed silicon photodetector for optical data link applications, IEEE Trans Electron Dev 43 (1996), 1054.
10. O.I. Dosunmu, D.D. Cannon, M.K. Emsley, L.C. Kimerling, and M.S. Ünlü, High-speed resonant cavity enhanced Ge photodetectors on reflecting Si substrates for 1550 nm operation, IEEE Photon Technol Lett 17 (2005), 175.
11. H.C. Luan, D.R. Lim, K.K. Lee, K.M. Chen, J.G. Sandland, K. Wada, and L.C. Kimerling, High-quality Ge epilayers on Si with low threading-dislocation densities, Appl Phys Lett 75 (1999), 2909.
12. M.S. Ünlü and S. Strite, Resonant cavity enhanced photonic devices, J Appl Phys 78 (1995), 607.
13. G.N. Milford, C.C. Harb, and E.H. Huntington, Shot noise limited ,microwave bandwidth photodetector design, Rev Sci Instrum 77 (2006), 114701.
14. L. Colace, P. Ferrara, G. Assanto, D. Fulgoni, and L. Nash, Low dark-current germanium-on-insulator near infrared detectors, IEEE Photon Technol Lett 19 (2007), 1813.
15. S.M. Sze, Physics of Semiconductor Devices, Wiley, New York, 1981.
16. B.W. Mullins, S.F. Soares, K.A. McArdle, C.M. Wilson, and S.R.J. Brueck, A simple high-speed Si Schottky photodiode, IEEE Photon Technol Lett 3 (1991), 360.
17. H.S. Dutta, N.R. Das, and M.K. Das, Investigating the effects of heterointerface trapping on the performance of Ge-based RCE Schottky photodiode at 1.55 μm, Sem Sc Technol 23 (2008), 085012.
18. N.R. Das and M.J. Deen, Calculating the photocurrent and transit-time-limited bandwidth of a heterostructure p-i-n photodetector, IEEE J Quantum Electron 37 (2001), 1574.
19. S.R. Forrest, Performance of $In_xGa_{1-x}AsyP_{1-y}$ photodiodes with dark current limited by diffusion, generation recombination and tunneling, IEEE J Quantum Electron 17 (1981), 217.

PLANAR TRIANGULAR MONOPOLE ANTENNA WITH MULTIOCTAVE BANDWIDTH

M. Naser-Moghadasi,[1] G. R. Dadashzadeh,[2] M. Abdollahvand,[2] Y. Zehforoosh,[1] and B. S. Virdee[3]

[1] Faculty of Engineering, Science and Research Branch, Islamic Azad University, Tehran, Iran; Corresponding author: mn.moghaddasi@srbiau.ac.ir

[2] Department of Electrical Engineering, Shahed University, Tehran, Iran

[3] Faculty of Computing, London Metropolitan University, London, United Kingdom

Received 30 March 2010

ABSTRACT: *This article presents the results of a novel triangular monopole antenna that exhibits multioctave performance. This modification significantly improves the antenna's impedance bandwidth by 167% over an ultrawideband frequency. The antenna's simulated return-loss and radiation patterns show very good correlation with the fabricated antenna's measured results.* © 2010 Wiley Periodicals, Inc. Microwave Opt Technol Lett 53:10–14, 2011; View this article online at wileyonlinelibrary.com. DOI 10.1002/mop.25673

Key words: *rectangular shape monopole antenna; small antenna; ultrawideband antenna*

1. INTRODUCTION

Ultrawideband (UWB) technology has undergone many significant developments in recent years. However, there still remain many challenges in making this technology live up to its full potential. The work in this area gained impetus with the Federal Communication Commission (FCC) permitting the marketing and operation of UWB products within the band 3.1–10.6 GHz. Commercial UWB systems require small low-cost antennas with

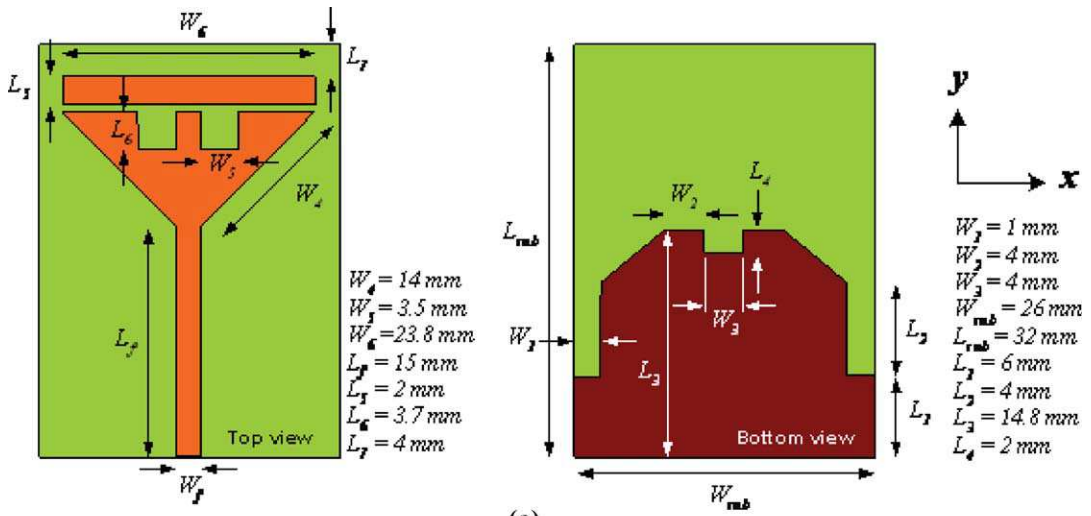

(a)

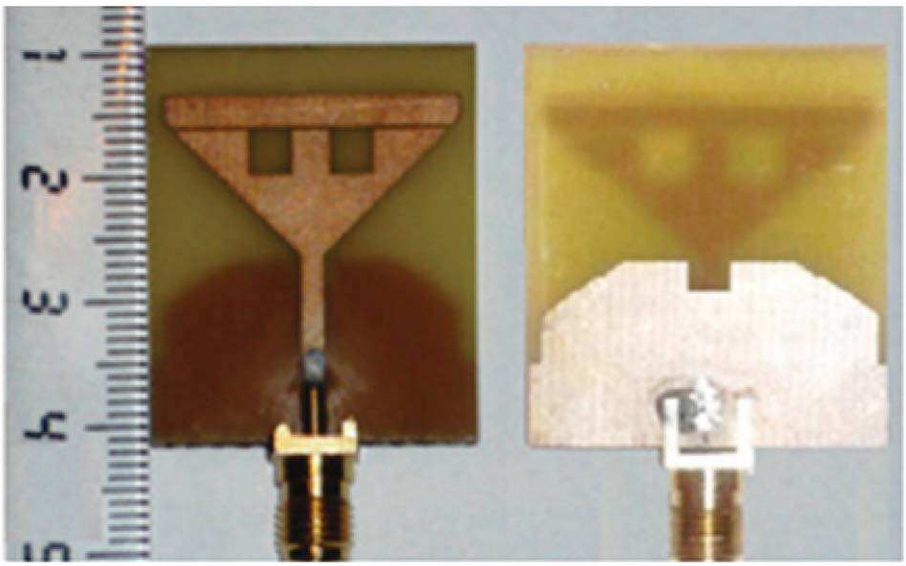

(b)

Figure 1 (a) Configuration and parameters defining the proposed antenna and (b) photograph of the fabricated antenna prototype. [Color figure can be viewed in the online issue, which is available at wileyonlinelibrary.com]

omni-directional radiation patterns, large bandwidth, and nondispersive behavior [1]. The planar monopole antenna is one of the candidate antennas, due to low-cost, broad bandwidth, and attractive profile [2–7]. The triangular monopole antenna mounted above a ground-plane was first proposed in [7], some variants of this type of antenna in an effort to increase its bandwidth have been studied [8, 9]. Although these techniques enhance the antenna's bandwidth, however, the results show their bandwidth is limited to less than 100%.

In this article, we present a novel planar microstrip-fed triangular monopole antenna that exhibits multioctave performance. The design of the proposed structure is based on the antenna presented in [10], but has a smaller size and a significantly large operational frequency band. The triangular monopole antenna includes notches above which is located a parasitic element in the form of a narrow rectangular-shaped patch. The antenna's ground plane is truncated and includes slits on the sides. This antenna designed operates over 3–33.5 GHz with $S_{11} < -10$ dB. Unlike other antennas reported in the literature to date, the proposed antenna displays a good omni-directional radiation pattern even at higher frequencies. The monopole antenna is analyzed using Ansoft's high-frequency simulator (HFSS^{TM}) [11]. Simulated and measured results are presented to validate the usefulness of the proposed antenna structure for UWB and multioctave applications.

2. ANTENNA STRUCTURE

Figure 1(a) shows the configuration of the proposed multioctave monopole antenna which consists of an inverted triangular structure whose base includes two square shaped notches, and positioned above triangular base is a parasitic rectangular resonant patch. The ground-plane is truncated, as shown in Figure 1(a), and envelops the feedline to the radiating triangular patch. The ground-plane includes a rectangular notch at its center and slits at its sides. The proposed antenna is constructed from FR4 substrate with thickness of 1.6 mm and relative dielectric constant of 4.4. The width W_f of the microstrip feedline is fixed at 2 mm. The antenna's dimensions are 26 mm $\times$ 32 mm ($L_{sub} \times W_{sub}$). The parameter $d = L_f - L_3$, represents the gap between the feed point to the triangular patch and the ground-plane. The dimensions of the notch ($L_4 \times W_3$) embedded in the ground-

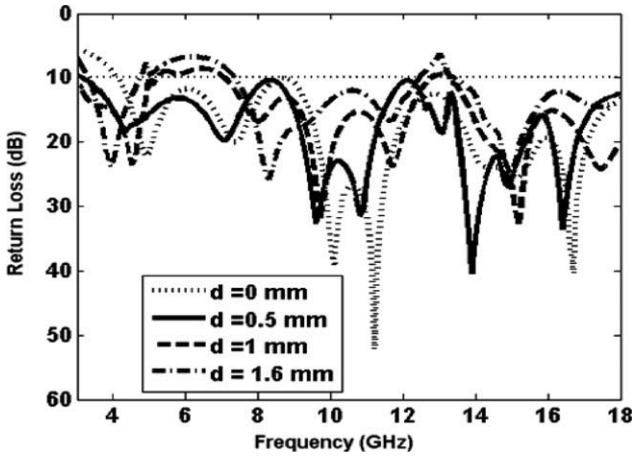

Figure 2 Simulated return-loss characteristics of a triangular patch antenna with different values of separation d

plane are important parameters in determining the sensitivity of the antenna's impedance match. The proposed shape of the truncated ground-plane acts as an effective impedance matching network to realize an antenna with a very wide impedance bandwidth. This is because the truncation creates capacitive loading that neutralizes the inductive nature of the patch to produce nearly pure resistive impedance present at the antenna's input [3]. The flare angle of the antenna also affects its impedance bandwidth. Here, the flare angle is set to be 90°. The narrow rectangular parasitic patch helps improve the return-loss characteristics ($S_{11} < -10$ dB) at the lower frequency band 3–4 GHz. Also, as will be shown in Section 3, by introducing slits in the sides of the ground plane and by carefully adjusting their dimensions results in improvement of the antenna's impedance match over 3–4 GHz and higher frequencies. By properly selecting the parameters of the slit dimensions ($L_2 \times W_1$), an impedance bandwidth of 11.2:1 can be realized. The improvement in impedance match over the multioctave bandwidth is attributed to the phenomenon of defected ground structure (DGS) with slits that creates additional surface current paths in the antenna. Moreover, this ground-plane structure changes the inductive and capacitive nature of the input impedance, which in turn leads to change in bandwidth [12]. The photograph of the prototype antenna is shown in Figure 1(b).

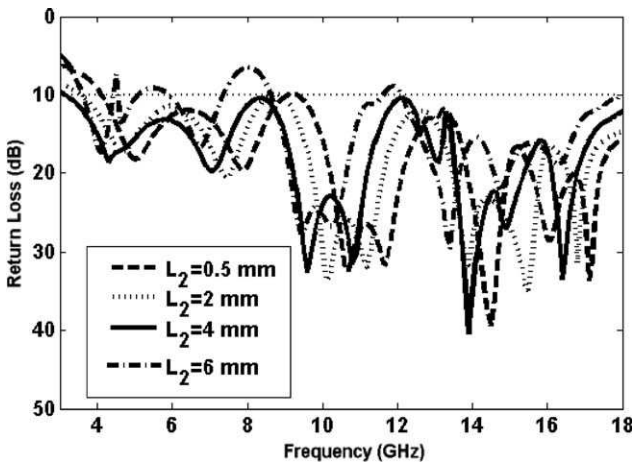

Figure 3 Simulated return-loss characteristics of the proposed antenna with different values of L_2 (W_1 is fixed at 1 mm)

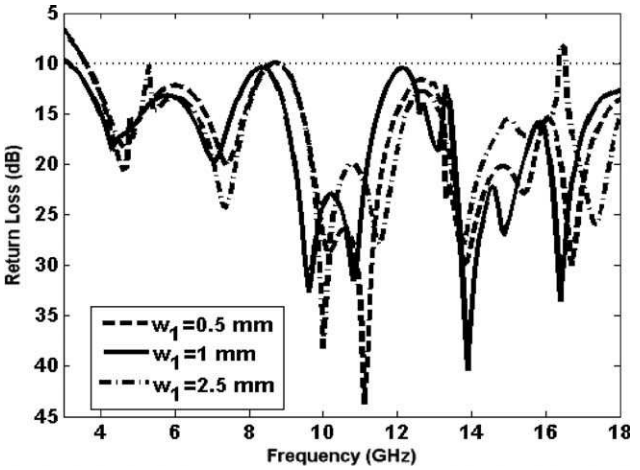

Figure 4 Simulated return-loss characteristics of the proposed antenna with different values of W_1 (L_2 is fixed at 4 mm)

3. RESULTS AND DISCUSSION

The proposed antenna is investigated by changing one parameter at a time, as fixing the others. To fully understand the behavior of the antenna's structure and to determine the optimum parameters, the antenna was analyzed using HFSS™. The optimum magnitudes of the physical parameters of the proposed antenna are shown in Figure 1(a).

The separation parameter $d = L_f - L_3$ is a parameter that has a major effect on the antenna's return-loss characteristics. By adjusting d, the electromagnetic coupling between the lower edge of the triangular patch and the ground-plane can be controlled. Figure 2 shows the return-loss response for different values of d. It is observed that the impedance bandwidth is effectively improved over the lower and upper frequencies as separation d is changed. It can be seen that the lower frequency of the impedance band is reduced by increasing the gap, but the impedance match becomes even poorer for larger values of d. This shows the sensitivity of the impedance match to this separation distance. As indicated above, the ground-plane serves as an impedance matching network, which is a function the separation distance d. The optimized separation distance d is 0.5 mm.

In this study, to enhance the impedance bandwidth characteristic, two symmetrical located rectangular slits are embedded in

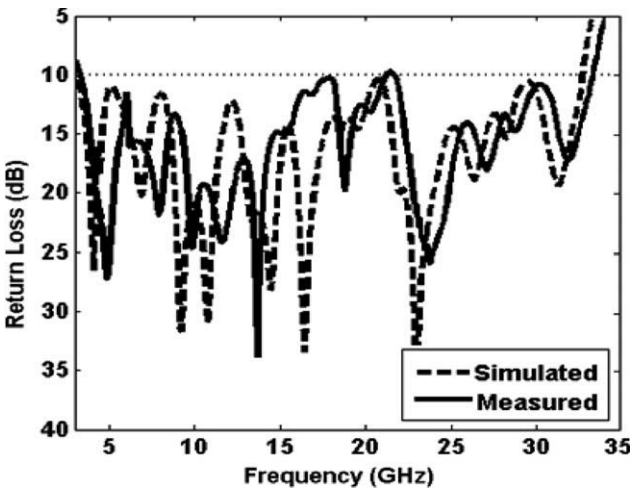

Figure 5 Simulated and measured return-loss response of the proposed antenna structure

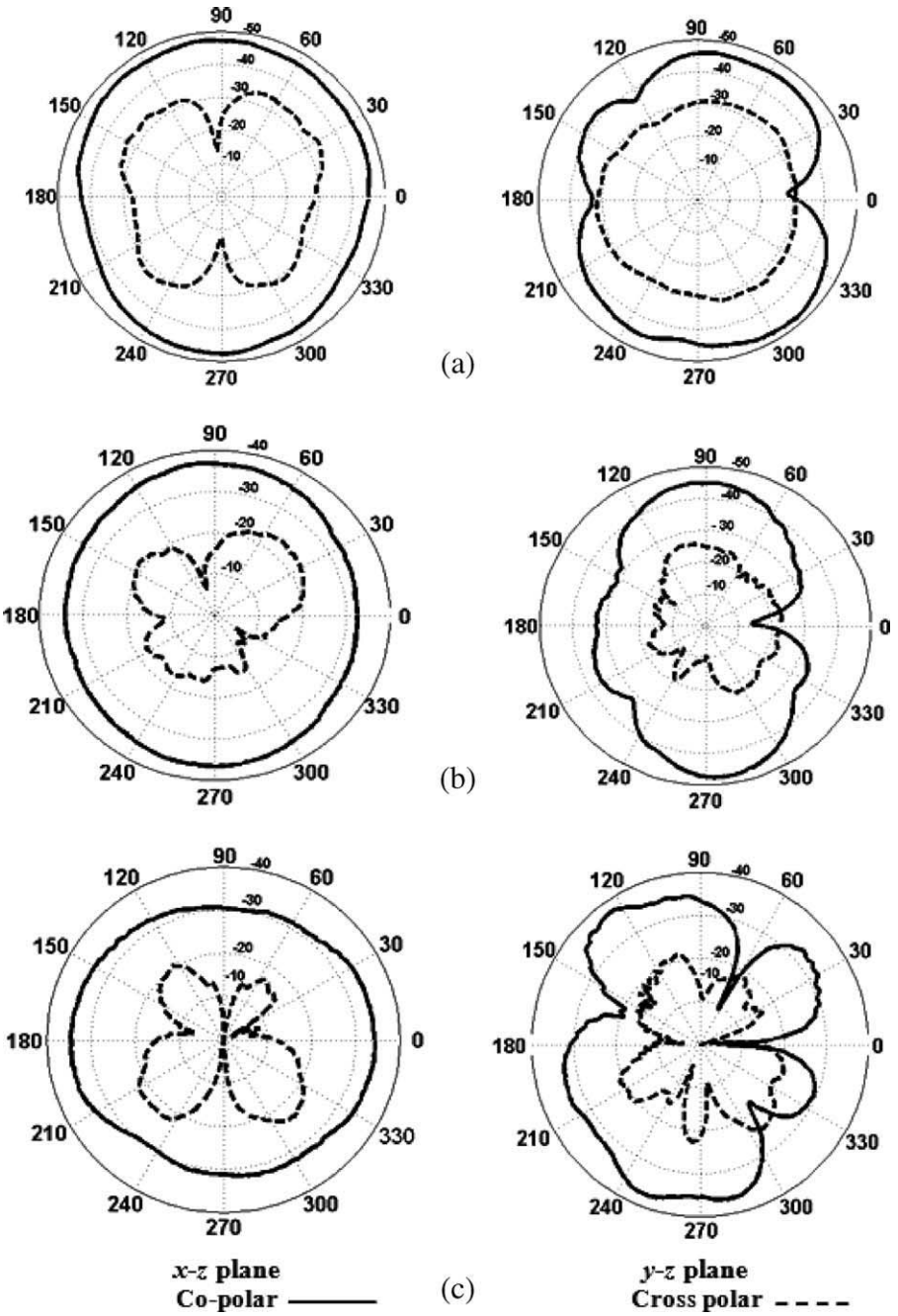

Figure 6 Measured radiation patterns of the proposed antenna in *x-z* and *y-z* plane at: (a) 4 GHz, (b) 7 GHz, and (c) 11 GHz

the ground plane of the proposed antenna, as depicted in Figure 1(a). Figures 3 and 4 show the return-loss response for several values of L_2 and W_1. These graphs indicate the importance of adding the pair of slits in the ground plane. It is found that the impedance bandwidth is greatly dependent on the dimensions of the slits ($L_2 \times W_1$). This phenomenon occurs because the slit acts as current perturbation on the ground-plane. These parameters are used to fine tune the impedance and determine the impedance bandwidth that can be achieved. The simulated return-loss responses with different values of L_2 are plotted in Figure 3. From the simulation results, it is found that the lower and upper frequencies are significantly affected by varying the slit length L_2. Also, the return-loss curves with the optimal slit length L_2 for various slit widths W_1 are plotted in Figure 4. It is observed that the impedance match is effectively changed by the varying the size of slit width. As the slit width is increased or decreased, the lower frequency of the return-loss response is affected. The slit width is a critical parameter to determine the lower and upper frequency of the impedance bandwidth. The optimum dimensions of the slit are $L_2 = 4$ mm and $W_1 = 1$ mm.

The impedance bandwidth was measured by using an Agilent 8722 Network Analyzer (50 MHz to 40 GHz). Figure 5 shows good agreement between the simulated and measured results. The disparity between the two responses is attributed to manufacturing tolerance and imperfect soldering effect of the SMA connector. The antenna's measured impedance bandwidth extends from 3 to 33.5 GHz for which its return-loss characteristic is better than -10 dB. This performance exceeds the UWB as defined by FCC.

Figure 6 shows the measured radiation patterns including the co-polarization and cross-polarization in the *H*-plane (*x-z* plane) and *E*-plane (*y-z* plane). It can be seen that the radiation patterns in *x-z* plane are nearly omnidirectional for the three frequencies.

4. CONCLUSIONS

In this article, a compact planar triangular monopole antenna is proposed that exhibits multioctave bandwidth performance and easily satisfies the requirements for UWB applications. The measured results show that the impedance bandwidth of the proposed antenna is significantly improved with the inclusion of square notches on the radiating patch, a narrow rectangular parasitic element located above the patch, and using a truncated ground-plane containing side slits. The measured results show good radiation patterns within the UWB frequency range.

REFERENCES

1. H. Schantz, The art and science of ultra wideband antennas, Artech House, Norwood, MA, 2005.
2. M. Ojaroudi, G. Kohneshahri, and J. Noory, Small modified monopole antenna for UWB application, IET Microwave Antennas Propag 3 (2009), 863–869.
3. A.A. Eldek, Numerical analysis of a small ultra wideband microstrip-fed tap monopole antenna, Prog Electromagn Res 65 (2006), 59–69.
4. J.W. Jung, W. Choi, and J. Choi, A compact broadband antenna with an L-shaped notch, IEICE Trans Commun E89-B (2006), 1968–1971.
5. Q. Wu, R. Jin, J. Geng, and J. Lao, Ultra-wideband rectangular disk monopole antenna with notched ground, Electron Lett 43 (2007), 1100–1101.
6. M. Abdollahvand and G.R. Dadashzadeh, Compact double-fed dual annular ring printed monopole antenna for UWB application, J Electromagn Waves Appl 23 (2009), 1969–1980.
7. G.H. Brown and O.M. Woodward, Experimentally determined radiation characteristics of conical and triangular antennas, RCA Rev 13 (1952), 425–452.
8. J.M. Johnson and Y. Rahmat-Samii, The tab monopole, IEEE Trans Antennas Propag 45 (1997), 187–188.
9. J.P. Lee, S.O. Park, and S.K. Lee, Bow-tie wideband monopole antenna with the novel impedance-bandwidth technique, Microwave Opt Technol Lett 36 (2002), 448–452.
10. C.C. Lin, H.R. Chuang, and Y.C. Kan, A 3–12 GHz UWB planar triangular monopole antenna with ridged ground-plane, Prog Electromagn Res 83 (2008), 307–321.
11. Ansoft Corporation. Ansoft high frequency structure simulation (HFSS), Version 10, Ansoft Corporation, Pittsburgh, PA, 2005.
12. A. Balalem, A.R. Ali, J. Machac, and A. Omar, Quasi-elliptic microstrip low-pass filters using an interdigital DGS slot, IEEE Microwave Wireless Compon Lett 17 (2007), 586–588.

DUAL-BAND FERRITE CHIP ANTENNA FOR GLOBAL POSITIONING SYSTEM AND BLUETOOTH APPLICATIONS

Seok Bae,[1] Yang Ki Hong,[1] Jae Jin Lee,[1] Ji Hoodn Park,[1] Jeevan Jalli,[1] Gavin S. Abo,[1] Won Mo Seong,[2] Sang Hoon Park,[2] Juk Sik Kum,[2] Won Ki Ahn,[2] and Gi Ho Kim[2]

[1] Department of Electrical and Computer Engineering and MINT Center, The University of Alabama, Tuscaloosa, AL 35487; Corresponding author: ykhong@eng.ua.edu

[2] EMW Co., Ltd., Seoul, South Korea

Received 30 March 2010

ABSTRACT: *Dual-band ferrite chip antenna having 105 mm^3 of volume was fabricated with $Ba_3Co_2Fe_{24}O_{41}$ (Co_2Z)-glass composite and antenna performance was evaluated. The permeability and permittivity of the composite were in the range of 1.92–2.12 and 7.33–7.45, respectively, from 1.575 to 2.45 GHz. Magnetic and dielectric loss tan δ of Co_2Z-glass composite was <3.5% in the 1.5–3.0 GHz range. The 3D average gain and bandwidth of the 40h-shake-milled and sintered Co_2Z-glass composite antenna were −1.27 dB and 355 MHz at 1.575 GHz, −4.08 dB and 270 MHz at 2.45 GHz, respectively. Simulated S-parameter spectrum is in good agreement with experimental results.*

DOI 10.1002/mop.25672

Key words: *dual band antenna; ferrite chip antenna; GPS; bluetooth; hexaferrite*

1. INTRODUCTION

Dual-band chip antenna was developed to work on both Global Positioning System (GPS; 1.575 GHz) and Bluetooth (BT; 2.45 GHz) for wireless handset. To miniaturize the dual band antenna to 100 mm^3 of the antenna volume, a radiator was embedded between two dielectric slabs. However, this embedded dielectric antenna shows low gain (GPS −2.6 dB, BT −2.4 dB) and narrow bandwidth (GPS 90 MHz, BT 130 MHz) [1]. However, the use of ferrite allows for achieving higher gain and broader bandwidth than the embedded dielectric antenna. Nonembedded radiator structure of ferrite antenna leads to better performance, while having the same volume of the embedded dielectric antenna. This is because the ferrite possesses both permeability and permittivity.

Recently, the low loss $Ba_3Co_2Fe_{24}O_{41}$ (Co_2Z) has been developed [2, 3] to miniaturize the VHF ferrite antenna [4]. To meet the GPS-BT dual-band frequencies, both magnetic and dielectric losses of the Co_2Z are needed to be low enough up to 2.45 GHz of the BT frequency. Therefore, the Co_2Z–glass composite was developed for use in the dual-band antenna. In this article, the dynamic properties of the developed low loss Co_2Z–glass composite and performance of the dual-band Co_2Z-glass composite chip antenna are reported.

2. EXPERIMENTAL

The Co_2Z-glass composite was used to fabricate the antenna substrate. The Co_2Z powder was prepared by the one-step mixing and calcination process [3]. Borosilicate glass powder was mixed with 40h-shake-milled Co_2Z powder. The ring shaped green bodies of the mixed powder were prepared by pressing with a steel mold and followed by sintering at 950°C for 1 h for dynamic magnetic characterization. Network analyzer (Agilent

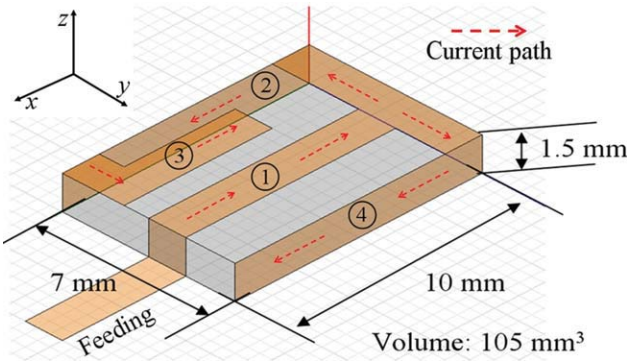

Figure 1 Structure and dimension of dual band ferrite chip antenna. [Color figure can be viewed in the online issue, which is available at wileyonlinelibrary.com]